Journal of Power Sources 616 (2024) 235143

Contents lists available at ScienceDirect

Journal of Power Sources

journal homepage: www.elsevier.com/locate/jpowsour

Fine-tuning thermal expansion characteristics of solid oxide fuel cell cathode via composite cathode fabrication

Nilam Shah [a], Tianjiu Zhu [a], Desheng Feng [a], Xiaoyong Xu [b,**], Fengli Liang [a], Hao Wang [c,d], Zhonghua Zhu [a,***], Lei Ge [c,d,*]

[a] School of Chemical Engineering, The University of Queensland, Brisbane, 4072, QLD, Australia
[b] School of Chemical Engineering, University of Adelaide, Adelaide, 5000, SA, Australia
[c] Centre for Future Materials, University of Southern Queensland, Springfield, QLD, 4300, Australia
[d] School of Engineering, University of Southern Queensland, Springfield, QLD, 4300, Australia

HIGHLIGHTS

- SOFC cathodes face durability issues from high thermal expansion.
- Negative thermal expansion material has been incorporated.
- Composite cathodes reduce the thermal expansion coefficient.
- The derived cathodes maintain activity and stability after thermal cycling.

GRAPHICAL ABSTRACT

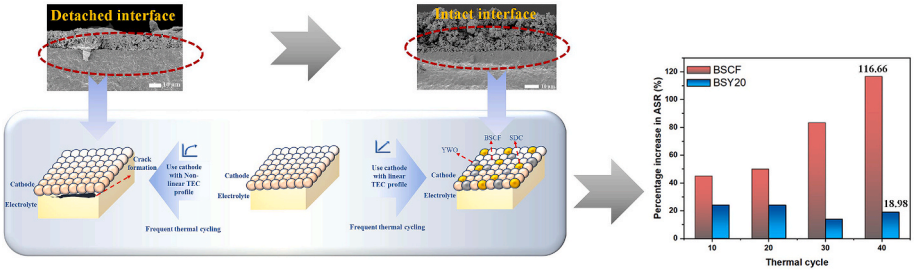

ARTICLE INFO

Keywords:
Solid oxide fuel cells
Durability
Thermal expansion coefficient
Composite cathode

ABSTRACT

Solid oxide fuel cells (SOFCs) offer promising prospects for sustainable electricity generation, attributed to high efficiency and fuel adaptability. However, their widespread application relies on three critical factors: performance, cost-effectiveness, and durability. Durability presents a significant hurdle; one key reason is the thermal expansion mismatch between cobalt-based cathodes and electrolytes, potentially leading to detachment at the cathode-electrolyte interface. In this study, we propose an approach to mitigate this challenge by fine-tuning the thermal expansion characteristics of the cathode. By tailoring lattice and chemical expansion, our composite cathode incorporates recognized materials like $Ba_{0.5}Sr_{0.5}Co_{0.8}Fe_{0.2}O_{3-\delta}$ with $Sm_{0.2}Ce_{0.8}O_{1.9}$ and the negative thermal expansion (NTE) material $Y_2W_3O_{12}$. Through the design of composite materials, we achieve enhanced thermal cycling stability with only ~20 % area-specific resistance (ASR) increases after 40 harsh thermal cycles between 300–600 °C compared to pure BSCF with over 100 % increment. This optimization process effectively reduces the thermal expansion coefficient while preserving BSCF's overall properties, offering a promising path for supporting SOFC durability and performance.

* Corresponding author.
** Corresponding author.
*** Corresponding author.
E-mail addresses: xiaoyong.xu@adelaide.edu.au (X. Xu), z.zhu@uq.edu.au (Z. Zhu), lei.ge@unisq.edu.au (L. Ge).

https://doi.org/10.1016/j.jpowsour.2024.235143
Received 22 April 2024; Received in revised form 15 July 2024; Accepted 26 July 2024
Available online 6 August 2024

1. Introduction

Solid oxide fuel cells (SOFCs) have emerged as a captivating choice for green energy solutions owing to their high efficiency, fuel flexibility, solid-state construction, invariant (solid) electrolyte, high-quality waste heat, and the absence of precious metals [1–4]. However, to fully realize their potential as a viable energy conversion technology, addressing critical challenges associated with their performance, cost-effectiveness, and durability is crucial. Durability is vital in ensuring the consistent and prolonged operation of SOFCs, which is essential for their widespread adoption [5]. However, the majority of the research in this field focused more on the performance enhancement of SOFCs through the development and designing of electrode materials such as $Ba_{0.5}Sr_{0.5}Co_{0.8}Fe_{0.2}O_{3-\delta}$ (BSCF) [6], $SrTa_{0.1}Nb_{0.1}Co_{0.8}O_{3-\delta}$ (STNC) [7], $SrSc_{0.175}Ta_{0.025}Co_{0.8}O_{3-\delta}$ (SSTC) [8], $SrNb_{0.1}Co_{0.9}O_{3-\delta}$ (SNC) [9], $SrCo_{0.8}Ti_{0.1}Ta_{0.1}O_{3-\delta}$ (SCTT) [10]. Cobalt-based perovskite gained a lot of attention due to its behaviour at intermediate temperatures lower than 700 °C [11–14], and though these materials behave better, they possess a higher thermal expansion coefficient [15]. Among the factors impacting durability, the thermal expansion mismatch between different components of SOFCs has significant implications.

Thermal expansion coefficient (TEC) values and their profiles can influence the performance of the SOFC system [16,17]. For instance, Rapid thermal cycling can hinder the application of SOFCs in mobile/-portable devices requiring quick start-up and shut-down capabilities [18]. Therefore, understanding and mitigating the impact of thermal expansion mismatch is critical for advancing the practical implementation of SOFCs in various applications. Delamination between functional layers, caused by thermal expansion mismatch and nonlinear TEC profile, is a challenge that compromises the durability and performance of SOFCs [19]. Delamination adversely affects the diffusion mechanism and increases overall resistance in the stack, leading to inconsistent and degraded performance outcomes [20]. Furthermore, the mismatch between the thermal expansion behaviours of the cathode and electrolyte materials and the sudden change in thermal expansion of the cathode, which led to thermal stress accumulation at the interface [21,22], is a primary contributor to delamination, further exacerbating the problem [23,24]. A study of SOFC based on ceria-based materials has shown that chemical expansion can have profound implications on delamination and vertical crack development in the layer itself [25]. However, chemical expansion relates to oxygen release and is directly proportional to oxygen release in the case of perovskites. To achieve better ORR activity, more oxygen vacancies and/or faster oxygen release are preferred. However, faster loss of lattice oxygen or sudden loss of lattice oxygen can be linked with the sudden increase in thermal expansion coefficient value at the temperature when the reduction reaction starts. This sudden change can create stresses in the electrode material itself and at the interface, which leads to cracking and delamination. So, it's critical to control chemical expansion along with lattice expansion with temperature changes.

To address these issues, the development of more robust and durable fuel cell systems is paramount. Researchers have focused on improving the thermo-mechanical compatibility between adjoined components to enhance the sustainability of SOFCs. Several strategies, such as A-site or B-site substitution [26,27], A-site deficiency creation [28,29], use of composite cathode by incorporating electrolyte material or NTE material into cathode material, etc. [26–28]. The later approach that has gained attention is the utilization of composite cathodes to improve thermal compatibility between the cathode and electrolyte. The thermal expansion behaviour of cathode materials, such as the widely studied cobalt-based perovskites, poses challenges due to their high TEC values [29]. Although Strontium cobaltite (SC) -type perovskites demonstrate excellent electrochemical behaviour, their practical applicability is hindered by the instability of their crystal structure at temperatures below 900 °C [30] and their high thermal expansion coefficients [31, 32].

Doping strategies involving A-site and B-site modifications have shown promise in improving the stability and oxygen reduction reaction (ORR) activity of these materials. However, this strategy does not always provide an optimum solution, as the electrochemical activity reduces with the decreasing concentration of Strontium and cobalt in the electrode material [33,34]. The substantial difference in TECs between the cathode materials and traditionally used electrolytes, such as Gadolinium-doped ceria (GDC), Yttria-stabilized zirconia (YSZ), and Samarium-doped ceria (SDC), exacerbates thermal incompatibility issues, leading to delamination between functional layers [35,36]. Other modification approaches also have limitations, such as limited deficiency creation to avoid structural instability [37,38] and limited addition of electrolyte or NTE content. In most cases, this limit might not be sufficient for tailoring the TEC of the cathode to a required value. The incorporation of composite materials with negative thermal expansion coefficients has proven effective in reducing thermal expansion in fuel cells and thermoelectric converters, where precise control of thermal expansion is critical [39]. Recently, researchers have extended this approach to the cathode materials of SOFCs [40–42]. The most important limitation of research in this area is that most strategies focused on overall thermal expansion with temperature and achieved a reduction in that value. However, chemical expansion is underestimated in terms of maintaining or improving electrochemical performance.

This paper aims to contribute to the development of durable SOFC systems by addressing the thermal expansion mismatch and its impact on cell performance. We propose an approach focusing on reducing lattice and chemical expansion. This involves fabricating composite cathodes to achieve reduced and gradual thermal expansion while preserving electrochemical behaviour. By incorporating NTE and electrolyte materials tailoring the TEC of perovskite cathode materials, we aim to improve thermal compatibility between the cathode and electrolyte. We investigate the composite cathode prepared using BSCF cathode, $Sm_{0.2}Ce_{0.8}O_{1.9}$ (SDC) electrolyte material, and $Y_2W_3O_{12}$ (YWO) as the NTE material. This study aims to analyse the potential of this approach, leading to comparable performance and improved durability. We selected BSCF as a cathode material for its outstanding performance at intermediate temperatures (around 600 °C) despite its thermal incompatibility with traditional electrolytes. The trade-off between catalytic activity and stability complicates electrode material development, making BSCF, a benchmark MIEC material, the ideal choice for this study. By addressing the challenges of thermal expansion mismatch, we aim to ensure sustained and efficient operation of SOFCs. Additionally, this strategy transforms BSCF from a theoretical concept into a practical solution, making this renowned material viable for real-world applications.

2. Experimental method

2.1. Sample synthesis

Phase-pure $Ba_{0.5}Sr_{0.5}C_{0.8}Fe_{0.2}O_{3-\delta}$ (BSCF) powder was synthesized using the sol-gel method, where stoichiometric amounts of nitrates were dissolved in water, a combination of EDTA and citric acid served as complexing agents, and an ammonia solution used to maintain the pH of the solution. Mild heating was applied to attain gelation of the solution, and then the resulting gel was heated at 250 °C for 12 h to remove organics. The obtained powder was calcined at 950 °C for 2 h in air. NTE material $Y_2W_3O_{12}$ was prepared using a solid-state reaction route. Ethanol was added into an appropriate amount of Y_2O_3 and WO_3; the mixture was ball-milled for 10 h at 300 Rpm. The mixture was air-dried in an oven at 80 °C and calcined at 1100 °C for 5 h in air. Commercialized electrolyte material $Sm_{0.2}Ce_{0.8}O_{1.9}$ (SDC) has been used as electrolyte material to prepare composite cathode powder and electrolyte disc. An appropriate amount of BSCF, SDC, and YWO has been mixed with the use of mortar and calcined at 950 °C for 2 h in the air to produce a composite cathode.

2.2. Fabrication of fuel cells

Electrolyte pellets having 495 μm thickness and 11 mm diameter were prepared using $Sm_{0.2}Ce_{0.8}O_{1.9}$(SDC), which is dry pressed at 4 Mpa and calcined at 1400 °C for 7 h in air. Composite cathode powder was dispersed in IPA (isopropyl alcohol) and glycerol, and then the mixture was ball milled at 300 Rpm for 2 h to produce cathode slurry. Then, the obtained cathode slurry was sprayed on both sides of the electrolyte disc, followed by calcination at 950 °C for 2h under an air atmosphere to acquire a symmetric cell configuration cathode\electrolyte\cathode.

2.3. Basic characterization

The crystal structure characterization of synthesized composite cathode powder has done by X-Ray Diffraction (XRD) to identify the crystalline structure of synthesized powder at room temperature, and patterns were recorded using the Bruker D8-Advanced X-Ray diffractometer using nickel-filtered Cu-Kα radiations. The samples were scanned under 40 kV and 40 mA in an angle range of $2\theta = 10°$ to 90° using a 0.1° for step increment. The XPS test was conducted using Kratos Axis Ultra spectrometric with AlKα (1486.8eV) radiation source at 150 W to understand surface chemistry and its effect. Data were analysed using CASAII software. Dense rectangular bar-shaped samples were formed by dry-pressing synthesized powders and fired at 1200 °C for 5h for BSCF and composite cathodes at 1150 °C for 20h in the air to observe thermal expansion. The temperature-programmed desorption (TPD) of oxygen was assessed utilizing the Micromeritics AutoChem II & HP apparatus. The specimens underwent a reduction in pure helium (50 mL/min), followed by the recording of TCD signals within the temperature range of 50–800 °C under a helium flow. The electrode material underwent thermal analysis through thermal gravimetric analysis using TGA, Q50 with a heating rate of 10 °C/min. The analysis was performed under flowing air (20 mL/min), starting from room temperature and progressing up to 800 °C. Surface morphology and the cathode/electrolyte interface were examined before and after a durability test using scanning electron microscopy (SEM) with a JEOL 7100 instrument. Additionally, transmission electron microscopy (TEM) imaging was performed using a field emission transmission electron microscope (HF5000) equipped with energy-dispersive X-ray spectroscopy (EDS) capabilities. The samples were prepared using an ethanol dispersion method and then mounted on a copper grid. A dense rectangular bar-shaped sample of the composite cathode BSY20 was formed by dry-pressing synthesized powders and fired at 1150 °C for 20h in the air to observe EDS using SEM Hitachi SU-3500.

2.4. Electrochemical test

Electrochemical impedance spectroscopy (EIS) was used to determine symmetrical cell polarization resistance (R_P) using the PGSTAT302 auto lab workstation. The EIS is carried out in a frequency range of 10000 Hz–0.1 Hz for a temperature range of 500–700 °C, where the air is used as fuel and flowrate kept at 150 mL/min for all tests. The difference between the lower and high-frequency intercepts on the real axis determined the R_p from the EIS spectra. Silver paste has been used as a current collector, and cells were connected using silver wires to enable connection with an external circuit.

3. Result and discussion

The schematic in Fig. 1a illustrates the configuration of the SOFC system employed in our study, highlighting the assembly of the cathode and electrolyte. The focus is on the effects of thermal expansion

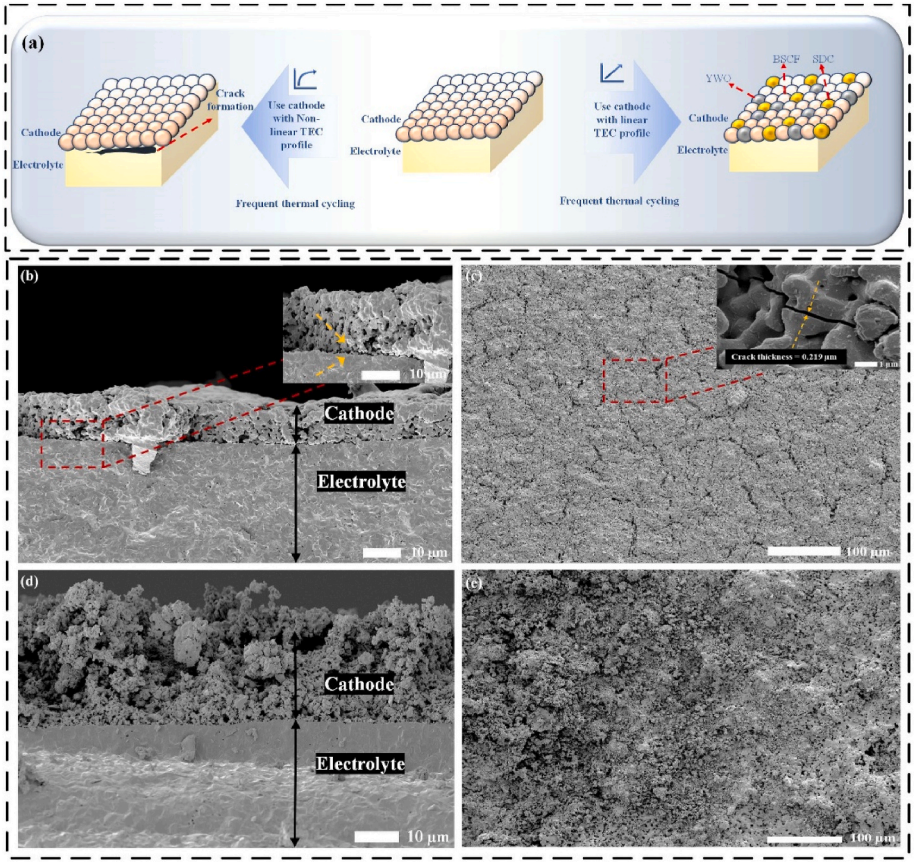

Fig. 1. (a) Schematic presentation of the experimental strategy, SEM analysis after durability test (b) Cross section of the interface of BSCF cathode and electrolyte (c) surface morphology of BSCF (d)Cross section of the interface of BSY20 composite cathode and electrolyte (e) surface morphology of BSY20.

mismatch and the nonlinear TEC profile between the pristine cathode and electrolyte materials. The schematic also represents the same configuration and its impact on the composite cathode developed in this study. This hypothesis is subsequently tested by assessing the pristine and composite cathode materials, specifically the BSY20 composite cathode synthesized in this study.

To explore this concept, five variants of composite cathodes were prepared, namely $Ba_{0.5}Sr_{0.5}Co_{0.8}Fe_{0.2}O_{3-\delta}$ (BSCF), (BSCF:YWO) (mass ratio = 100:10)) (BY10), (BSCF:YWO (mass ratio = 100:20)) (BY20), (BSCF:SDC:YWO (mass ratio = 100:20:10)) (BSY10), and (BSCF:SDC:YWO (mass ratio = 100:20:20)) (BSY20). The choice of 20 % SDC incorporation was based on a previous study [43], suggesting it as an optimum level to enhance the triple phase boundary (TPB) and provide more reactive sites. Additionally, SDC is known to be effective at lower temperatures [44]. However, excessive loading of electrolyte material might lead to agglomeration, potentially interfering with diffusion and affecting the oxygen reduction reaction (ORR) mechanism.

The study considers the balance between electrolyte and NTE material in the composite cathode, focusing on maintaining the optimum amount of SDC and NTE material YWO. The addition of YWO aims to balance the thermal expansion coefficient of the composite cathode, as demonstrated in previous research [45]. The interaction between the cathode and YWO introduces A-site deficiency, improving performance. However, an excess of NTE material may lead to a more significant A-site deficiency, potentially deteriorating cell performance due to a shift in the rate-determining step from oxygen surface diffusion to charge-transfer processes [46]. Hence, this research was conducted to maintain the optimal concentration of electrolyte (SDC) and NTE material (YWO) within the composite cathode and evaluate the synergistic effects arising from the addition of SDC and YWO. The study systematically assesses the compatibility of BSCF, SDC, and YWO, investigating their influence on the electrochemical and thermal characteristics of the synthesized composite cathode to determine the viability of this material.

To validate our hypothesis, scanning electron microscopy (SEM) analysis was conducted on the cathode materials after undergoing durability tests. Durability tests were carried out by frequent thermal cycling to both materials. SEM images after thermal cycling tests are presented for the interface of BSCF/SDC, Surface analysis of BSCF cathode, the interface of BSY20/SDC, and surface analysis of BSY20 in Fig. 1 b, c, d, & e, respectively. The SEM results confirm the correctness of our hypothesis and reveal significant insights. In the pristine cathode material, numerous cracks are observed, indicating the occurrence of mechanical stress and strain during thermal cycling. A similar occurrence was noted in the microstructural alterations and performance decline of BSCF during prolonged operation in electrolysis mode [47]. These cracks can compromise the overall performance and stability of the material. Furthermore, detachment between the cathode and electrolyte is evident, highlighting the vulnerability of the pristine cathode material to degradation and delamination under thermal cycling conditions. In contrast, the composite cathode material demonstrates improved structural integrity. SEM analysis reveals a limited occurrence of cracks and reduced detachment between the cathode and electrolyte. This signifies the ability of the composite cathode material to withstand the mechanical stresses associated with thermal cycling. Consequently, the composite cathode exhibits enhanced thermal cycle resistance and long-term durability in SOFC applications. The improved durability and reduced occurrence of cracks and detachment validate the effectiveness of the composite cathode in addressing the thermal expansion mismatch issue and enhancing the long-term stability of SOFCs.

The outcomes of the durability test highlight the potential of the composite cathode material to enhance the long-term performance and reliability of SOFCs under varying temperature conditions. Specifically, Fig. 2a illustrates that BSY20 exhibits a lower thermal expansion coefficient (TEC) and more gradual expansion behaviour compared to BSCF. This reduction in TEC, particularly within the operating temperature range, contributes significantly to improved thermal cycle resistance. BSY20 demonstrates a TEC of $(12.81 \pm 0.41) \times 10^{-6}\ K^{-1}$ within the temperature range of RT-800 °C, in contrast to the pristine cathode material's TEC of $(20.92 \pm 0.68) \times 10^{-6}\ K^{-1}$ in the same temperature

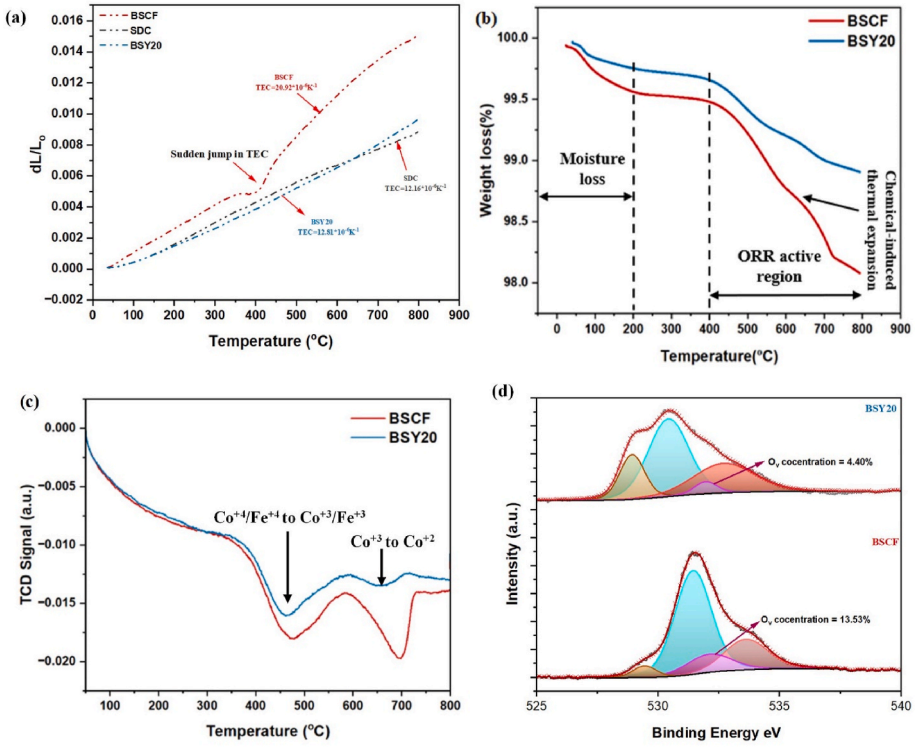

Fig. 2. (a) Thermal expansion of BSCF, BSY20, and SDC in the air for temperature range RT-800 °C (b) thermogravimetric analysis for BSCF and BSY20 (c) O2-TPD profiles for BSCF and BSY20 (d) XPS analysis of O1s for BSCF and BSY20.

range. The reduced thermal expansion of the composite cathode material results in minimized stress and strain accumulation during thermal cycling, mitigating the risk of mechanical failures, such as cracking or delamination, that could adversely affect cathode performance and stability.

The incorporation of electrolyte and NTE components in the composite cathode material achieves a more balanced and controlled thermal expansion response. Literature suggests that chemical expansion occurs due to cobalt ion spin transition, thermal/chemical reduction of cobalt ions to lower oxidation states [48], and the release of more oxygen [49]. As presented in Fig. 2b, the higher thermal expansion observed in BSCF, particularly after reaching a temperature of 400 °C, is primarily attributed to the increased release of oxygen. The TGA data depicted in Fig. 2b under an air atmosphere indicate that BSY20 experiences a lesser release of lattice oxygen compared to BSCF. This reduction in chemical expansion may contribute to performance stability during thermal cycling, enhancing the overall thermal stability of the composite cathode material.

The TEC of the BSCF perovskites is closely linked to the effects of chemical expansion resulting from variations in the concentration of point defects and the spin state of cobalt ions [50]. Fig. 2c illustrates the Temperature-Programmed Oxygen Desorption (O_2–TPD) curves obtained for BSCF and BSY20. Two distinct onset temperatures, approximately 300 °C and 800 °C, indicate oxygen desorption, referred to as α- and β-oxygen desorption. BSCF exhibits significant desorption peaks in the intermediate-temperature range of 300–600 °C (α-peak) and the range of 700–900 °C (β-peak), consistent with previous literature [46,51]. These peaks correspond to the reduction of Co^{+4}/Fe^{+4} to Co^{+3}/Fe^{+3} and Co^{+3} to Co^{+2}, respectively [46]. The reduction in peak intensity implies a decreased conversion of cobalt and/or iron from higher oxidation states to lower oxidation states, ultimately resulting in a reduction in chemical expansion. When BSCF, SDC, and YWO interact at elevated temperatures, it alters the valence state of the B-site cation, allowing for a reduction in chemical expansion. Our selection of materials and optimal loading result in the BSY20 composite cathode achieving a balance between thermal and electrochemical properties.

Table 1 overviews the oxygen component concentrations for BSCF and BSY20, indicating the presence of lattice O^{2-}, $O_2{}^{2-}/O^-$, oxygen vacancies (O_v), and water (H_2O). Surface analysis through X-ray Photoelectron Spectroscopy (XPS) supports the dilution of BSCF by confirming a low oxygen vacancy concentration in the composite cathode. The O1s spectra in the region of 525–540 eV reveal distinct peaks, representing lattice oxygen species, oxygen vacancies, surface oxidative oxygen or adsorbed O_2, and the presence of water on the surface [52] for both BSY20 and BSCF. Comparing the O1s spectra of BSY20 and BSCF, a lower concentration of oxygen vacancies (Ov) is evident in BSY20, aligning with the slight increase in ASR value and activation energy of composite cathode as explained in the following section. The reduction in oxygen vacancy concentration can be attributed to the dilution of BSCF material in the composite cathode material prepared using BSCF, SDC, and YWO, as BSCF has higher oxygen vacancy.

The X-ray diffraction (XRD) patterns for BSCF and its composites with YWO (negative thermal expansion material) and SDC (electrolyte material) were recorded at room temperature after mixing and sintering at 950 °C for 2 h in air. These patterns are shown in Fig. 3a, with additional data in Supporting Information Figure S1. To optimize the calcination temperature for the composite cathode powders, we conducted XRD analysis of BY10 at 800 °C, 950 °C, and at room temperature. Significant lattice shrinkage at 950 °C, indicated by the main peak shifting towards higher angles, led us to select 950 °C as the optimal calcination temperature to achieve favorable thermal expansion properties with SDC. The $BSWO_4$ phase formed at both temperatures. Fig. S2a presents XRD data for BSCF, BY10_RT (BY10 composite cathode without calcination), BY10_800 (BY10 composite cathode calcined at 800 °C for 2h), and BY10_950 (BY10 composite cathode calcined at 950 °C for 2h). Fig. S2b provides zoomed-in sections illustrating greater lattice shrinkage at 950 °C, justifying its selection. This ensures the composite cathode maintains structural integrity and performance under operational conditions.

Table 1
Oxygen components concentration for BSCF and BSY20.

Cathode material	lattice O^{2-}	$O_2{}^{2-}/O^-$	Oxygen vacancy	H_2O
BSCF	4.38 % ± 0.44 %	60.78 % ± 6.08 %	13.53 % ± 1.35 %	21.31 % ± 2.13 %
BSY20	17.72 % ± 1.77 %	49.90 % ± 5 %	4.40 % ± 0.44 %	27.98 % ± 2.80 %

The chemical compatibility of BSCF and SDC persists up to 900 °C, with negligible reactions reported [43]. Calcination of the BSY20 composite at 950 °C reveals an additional phase, $BaSrCeO_3$, evidenced by a minor shoulder peak at 28.8° 2θ in the XRD pattern, though challenging to confirm due to overlapping with another peak at the same value. HRTEM analysis in Supplementary Fig. S7 confirms the presence of the extra phase barium strontium tungstate (BSWO) in composites, indicating a chemical reaction between BSCF and YWO. The reaction involving A-site cations Ba and Sr induces A-site deficiency in the BSCF structure. A-site deficiency creates an extra oxygen vacancy to maintain charge balance for A-site deficient BSCF [46,53]. Surprisingly, our developed material shows no additional oxygen vacancies; instead, a reduction in oxygen vacancy content is observed in the composite material. This reduction is attributed to the dilution of BSCF in composite material.

Fig. 3b magnifies the diffraction for the main peak of BSCF in BSCF and BSY20. Composites BY10, BY20, BSY10, and BSY20 exhibit a shift to a higher angle value of 2θ, indicating lattice shrinkage. The presence of YWO influences the TEC value, as illustrated in Fig. 2a. The formation of additional phases in a composite material results in the establishment of chemical bonds between all three base materials, potentially enhancing cohesion and overall performance. High-Resolution Transmission Electron Microscopy (HRTEM) analysis at a selected site in Fig. 3c confirms the coexistence of all base phases (BSCF, SDC, and YWO), as shown in Fig. 3d. STEM analysis, combined with elemental mapping, confirms the presence of all expected elements in the structure (Fig. S9), including barium, strontium, cobalt, iron, cerium, samarium, yttrium, tungsten, and oxygen. The high intensity of samarium, cerium, and oxygen indicates that the selected EDS area contains a significant quantity of SDC, suggesting that SDC remains largely unreacted with other materials in the composite. This observation also points to a degree of chemical compatibility between SDC and the other composite components. The presence of other elements at lower intensities suggests their incorporation into the matrix, verifying the successful integration of all constituents within the composite. We prepared a bar-shaped pellet to achieve a broader coverage for EDS and facilitate a smooth surface suitable for EDS analysis. As anticipated, the subsequent SEM-EDS analysis revealed a uniform distribution of all metals on the microscale.

Reduced cobalt and iron reduction leads to decreased chemical expansion, potentially impacting electrochemical reactions and Oxygen Reduction Reaction (ORR) activity. However, adding Solid Electrolyte material (SDC) extends the triple-phase boundary (TPB) [54,55], improving diffusion and maintaining electrochemical activity comparable to BSCF, with increased cathode thickness (33 μm). The formation of the new phase BSWO does not compromise performance.

To evaluate electrochemical activity, both materials were tested under air in a symmetric cell configuration. Electrochemical Impedance Spectroscopy (EIS) results (Fig. 4a) show that the pristine BSCF and the composite cathode achieve comparable Area-Specific Resistance (ASR) values. At 600 °C, BSCF exhibits an ASR of 0.058 ± 0.006 Ω cm^2, while the composite cathode shows 0.074 ± 0.003 Ω cm^2. Despite a slight difference, the composite cathode's performance remains promising, indicating suitable electrochemical activity for SOFC applications.

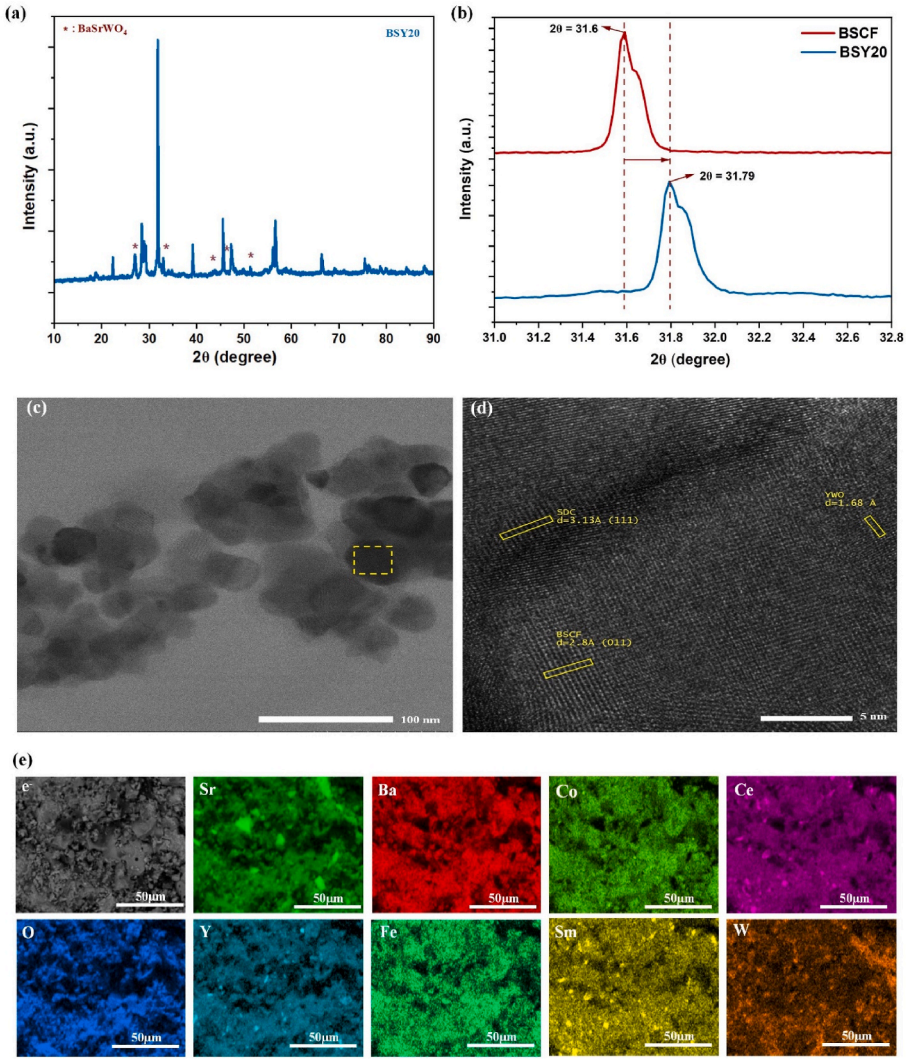

Fig. 3. (a) X-ray diffraction plot for composite cathode material BSY20 (b) Magnified XRD data section for the range between 2θ = 31–32.8-degree (c) STEM and (d) corresponding HRTEM image of the interfaces of BSCF, SDC and YWO for BSY20 (e) SEM-EDS analysis of BSY20.

The reduced oxygen vacancy content observed in TGA and XPS data does not significantly impact electrochemical performance. Impedance tests show comparable ASR for BSY20 to BSCF. The inclusion of SDC extends the TPB, providing more reactive sites, while unreacted YWO does not participate in ORR (supporting info Fig. S3). In the BSY20 composite, YWO reacts with BSCF to form BSWO, with yttrium likely occupying the B-site of BSCF. This is suggested by the peak shift in XRD data (Fig. 3b) and confirmed by EDS analysis (Fig. 3e) showing yttrium distribution. The comparable ORR performance is attributed to TPB extension and B-site yttrium incorporation, which enhances performance and provides structural stability to BSCF, mitigating the impact of BSCF dilution with YWO and SDC.

The stability of the symmetric cell with BSY20 in air was evaluated at 600 °C over a span of approximately 200 h under open circuit conditions. Throughout the test, a consistently low value of ASR was observed, as depicted in Fig. 4b, with an initial ASR of 0.064 Ω cm^2 and a final ASR of 0.079 Ω cm^2. We also evaluated the long-term structural stability of the BSY20 composite cathode material. The material underwent a prolonged heat treatment at 600 °C for 200 h. Post-treatment XRD analysis showed no additional peak formation, indicating the preservation of the original structure. This stability suggests that the structural integrity of the composite material is maintained, which correlates with the consistent electrochemical performance observed during the extended testing period. XRD results are presented in the Supporting Information as Fig. S10. This finding emphasizes the reliability of the composite material for long-term applications in SOFCs.

A spider chart analysis in Fig. 4c evaluates thermally and electrochemically controlled performance parameters. The results indicate that the prepared composite cathode material is a balanced choice for performance across various criteria. The addition of electrolyte material contributes to extending TPB, while the presence of the NTE component provides a compensating effect, counteracting excessive expansion. This combined approach effectively mitigates thermal expansion mismatch between the cathode material and other cell components, reducing the risk of thermo-mechanical stress and enhancing the material's ability to withstand thermal cycling.

As presented in Fig. 4d, the evaluation of thermal cycle resistance in the composite cathode material BSY20, incorporating electrolyte and NTE components, was compared to the pristine cathode material BSCF. The increase in measured ASR after multiple thermal cycles provided insights into performance degradation and thermal cycle stability. The pristine cathode material exhibited a significant increase in ASR from 0.060 to 0.13 Ω cm^2, indicating reduced stability and degradation with each subsequent thermal cycle. In contrast, BSY20 exhibited a lower increase in ASR, rising from 0.079 to 0.098 Ω cm^2 after 10 thermal cycles and remaining consistent up to 40 thermal cycles. To demonstrate the feasibility of using a thicker electrode in the composite cathode, we intentionally increased the thickness when incorporating SDC, which

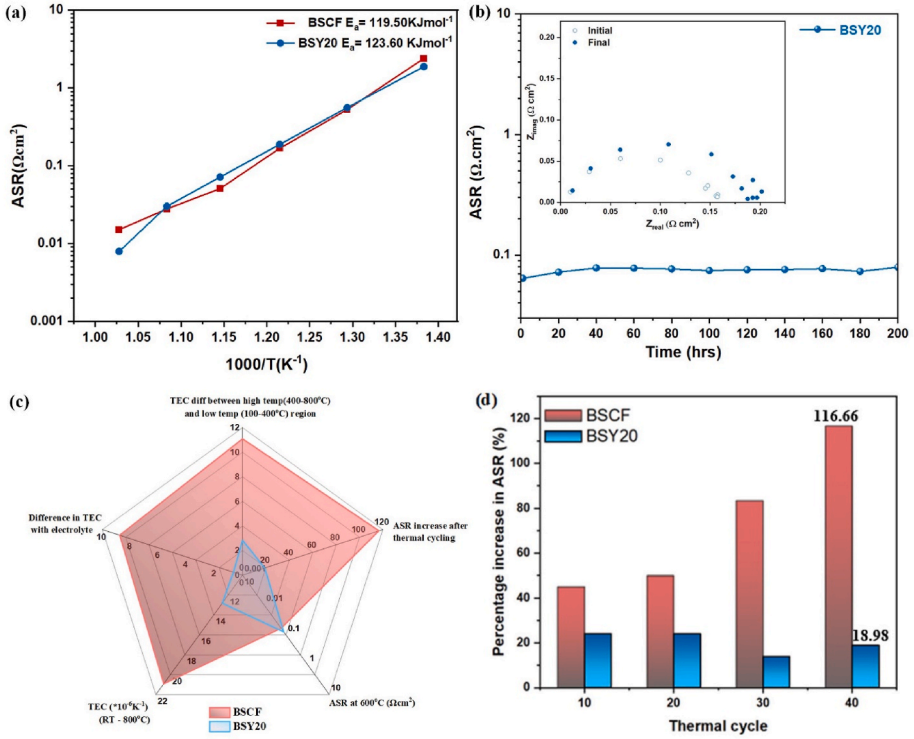

Fig. 4. (a) Temperature dependence on ASR of BSCF and BSY20 (b) stability test for BSY20 at 600 °C in air (C) spider chart analysis for BSCF and BSY20 for thermal stability (d) ASR response on symmetric cells using BSCF and BSY20 cathode materials during thermal cycling with a heating rate of 30 °C/min and passive cooling between the temperature range of 600–300 °C.

extends the TPB. This extension results in a more robust and thicker electrode. Conversely, a similarly thick BSCF electrode would experience delamination during thermal cycling owing to its higher TEC [56, 57], complicating reliable material testing. To avoid these issues, the BSCF layer was maintained at a thickness of 10–15 μm. This approach ensures a fair comparison while preserving the integrity of the BSCF and showcasing the enhanced stability of the SDC-incorporated composite cathode. Literature supports that thicker composite cathodes perform better electrochemically [45,58–60].

This result explains improved thermal cycle resistance and enhanced durability compared to the pristine cathode material. The stabilization of ASR in the composite cathode material reflects its ability to maintain performance and stability throughout subsequent thermal cycles. The incorporation of electrolyte and NTE components in the composite cathode formulation effectively mitigates the detrimental effects of thermal cycling on the cathode material.

In summary, the composite cathode comprises three components: perovskite BSCF, electrolyte SDC, and negative thermal expansion material YWO. These components have different thermal expansion behaviors, and their distribution within the composite cathode significantly impacts the overall thermal expansion coefficient (TEC) and potential for microcracking under thermal cycling. However, the interaction between BSCF and YWO leads to the formation of an integrated structure. The contact structure among BSCF, YWO, BSWO, and SDC can self-reconstruct through mechanisms such as pore-filling and topology changes [45], which enhances stability and prevents internal delamination. Although this interphase formation may appear to dilute the perovskite phase, it helps maintain structural integrity and reduce chemical expansion by distributing the BSCF more evenly.

Additionally, the literature has demonstrated that the incorporation of materials like YWO enhances the thermal and mechanical stability of composite cathodes. The formation of strong interphase boundaries and the minimization of TEC mismatch are critical in mitigating issues related to thermal cycling and chemical expansion. To further address these concerns, we conducted X-ray diffraction (XRD) tests after long-term heat treatment to observe structural changes. These tests show that our composite material maintains structural stability over extended periods, supporting the reliability of our approach.

4. Conclusion

The composite cathode design, comprising BSCF, SDC, and YWO in a 100:20:20 mass ratio, aimed to maintain thermomechanical strength and durability under operating conditions. Fabricated through sintering at 950 °C, the composite cathode, labelled BSY20, exhibited resistance to thermal cycling and sustained stability. Compared to pristine cathode BSCF, BSY20 displayed superior performance, with only a 24 % increase in ASR after 10 thermal cycles and consistent behaviour up to 40 cycles (19 % ASR increase). Notably, BSY20 avoided delamination between the electrolyte and cathode, maintaining integrity with the electrolyte surface. Morphological examination post-durability testing confirmed BSY20's intactness, supporting its enhanced durability. These findings emphasize BSY20's potential as a promising cathode material for intermediate-temperature SOFCs, offering optimized electrochemical performance and superior durability for practical application. The successful integration of BSCF, SDC, and YWO in the composite cathode demonstrates a synergistic solution to thermal cycling and material stability challenges, advancing SOFC technology.

CRediT authorship contribution statement

Nilam Shah: Writing – review & editing, Writing – original draft, Methodology, Investigation, Formal analysis, Data curation. **Tianjiu Zhu:** Formal analysis, Data curation. **Desheng Feng:** Formal analysis, Data curation. **Xiaoyong Xu:** Writing – review & editing, Writing – original draft, Supervision, Project administration, Methodology. **Fengli Liang:** Supervision, Methodology. **Hao Wang:** Writing – original draft, Resources, Project administration, Investigation. **Zhonghua Zhu:**

Writing – review & editing, Writing – original draft, Supervision, Resources, Project administration, Investigation, Funding acquisition, Conceptualization. **Lei Ge:** Writing – review & editing, Writing – original draft, Supervision, Resources, Project administration, Funding acquisition, Conceptualization.

Declaration of competing interest

The authors declare that they have no known competing financial interests or personal relationships that could have appeared to influence the work reported in this paper.

Data availability

Data will be made available on request.

Acknowledgement

N Shah would like to thank the RTP research scholarship from the University of Queensland. ZH Zhu and H Wang would like to thank the financial siupport from Australian Research Council Discovery Project DP190101782. L Ge wants to thank the financial support from ARC Future Fellowship project FT220100166.

Appendix A. Supplementary data

Supplementary data to this article can be found online at https://doi.org/10.1016/j.jpowsour.2024.235143.

References

[1] L. Fan, B. Zhu, P.-C. Su, C. He, Nano Energy 45 (2018) 148–176.
[2] Y. Song, Y. Chen, W. Wang, C. Zhou, Y. Zhong, G. Yang, W. Zhou, M. Liu, Z. Shao, Joule 3 (2019) 2842–2853.
[3] Y. Sahli, H. Ben Moussa, B. Zitouni, Int. J. Hydrogen Energy 44 (2019) 22445–22454.
[4] X. Xu, X. Han, Y. Zheng, W. Zhou, K. Davey, S.-Z. Qiao, Chem Catal. (2023) 100794.
[5] R.S. Krishnan, R. Srinivasan, S. Devanarayanan, B.R. Pamplin, Thermal Expansion of Crystals: International Series in the Science of the Solid State, Elsevier Science, 2013.
[6] Z. Shao, S.M. Haile, Nature 431 (2004) 170–173.
[7] M. Li, M. Zhao, F. Li, W. Zhou, V.K. Peterson, X. Xu, Z. Shao, I. Gentle, Z. Zhu, Nat. Commun. 8 (2017) 13990.
[8] X. Xu, J. Zhao, M. Li, L. Zhuang, J. Zhang, S. Aruliah, F. Liang, H. Wang, Z. Zhu, Compos. B Eng. 178 (2019) 107491.
[9] V. Cascos, R. Martínez-Coronado, J.A. Alonso, Int. J. Hydrogen Energy 39 (2014) 14349–14354.
[10] H. Gu, M. Xu, Y. Song, C. Zhou, C. Su, W. Wang, R. Ran, W. Zhou, Z. Shao, Compos. B Eng. 213 (2021) 108726.
[11] Y. Liu, J. Chen, F. Liang, J. Pu, B. Chi, L. Jian, Int. J. Hydrogen Energy 38 (2013) 6802–6808.
[12] C. Sun, J.A. Alonso, J. Bian, Adv. Energy Mater. 11 (2021) 2000459.
[13] Y.A. Mastrikov, M.M. Kuklja, E.A. Kotomin, J. Maier, Energy Environ. Sci. 3 (2010) 1544–1550.
[14] R. Vinoth Kumar, A.P. Khandale, Renew. Sustain. Energy Rev. 156 (2022) 111985.
[15] T. Wei, Q. Zhang, Y.-H. Huang, J.B. Goodenough, J. Mater. Chem. 22 (2012) 225–231.
[16] Y. Zhang, C. Xia, J. Power Sources 195 (2010) 6611–6618.
[17] Y. Niu, W. Lv, K. Wen, X. Shi, R. Luo, W. He, Solid State Ionics 311 (2017) 63–68.
[18] Z. Shao, S.M. Haile, J. Ahn, P.D. Ronney, Z. Zhan, S.A. Barnett, Nature 435 (2005) 795–798.
[19] K. Park, S. Yu, J. Bae, H. Kim, Y. Ko, Int. J. Hydrogen Energy 35 (2010) 8670–8677.
[20] T. Yang, Y. Fan, J. Liu, H. Finklea, S. Lee, B. Guan, H.W. Abernathy, T.L. Kalapos, G.A. Hackett, Int. J. Hydrogen Energy 47 (2022) 41124–41137.
[21] N.P. Padture, M. Gell, E.H. Jordan, Science 296 (2002) 280–284.
[22] X. Liu, H. Wang, W. Wang, Z. Fu, J. Solid State Chem. 299 (2021) 122111.
[23] D. Wachsman Eric, T. Lee Kang, Science 334 (2011) 935–939.
[24] W. Zając, K. Świerczek, J. Molenda, J. Power Sources 173 (2007) 675–680.
[25] K. Sato, K. Yashiro, T. Kawada, H. Yugami, T. Hashida, J. Mizusaki, J. Power Sources 195 (2010) 5481–5486.
[26] A. Eksioglu, L. Colakerol Arslan, M. Sezen, C. Ow-Yang, A. Buyukaksoy, ACS Appl. Mater. Interfaces 11 (2019) 47904–47916.
[27] E. Perry Murray, S.A. Barnett, Solid State Ionics 143 (2001) 265–273.
[28] M. Zhang, G. Jeerh, P. Zou, R. Lan, M. Wang, H. Wang, S. Tao, Mater. Today 49 (2021) 351–377.
[29] N. Li, Z. Lü, B. Wei, X. Huang, K. Chen, Y. Zhang, W. Su, J. Alloys Compd. 454 (2008) 274–279.
[30] H. Kruidhof, H.J.M. Bouwmeester, R.H.E.v. Doorn, A.J. Burggraaf, Solid State Ionics 63–65 (1993) 816–822.
[31] N. Shah, X. Xu, J. Love, H. Wang, Z. Zhu, L. Ge, J. Power Sources 599 (2024) 234211.
[32] Y. Cheng, Q. Zhou, W. Li, T. Wei, Z. Li, D. An, X. Tong, Z. Ji, X. Han, J. Alloys Compd. 641 (2015) 234–237.
[33] Y. Teraoka, H.-M. Zhang, S. Furukawa, N. Yamazoe, Chem. Lett. 14 (1985) 1743–1746.
[34] K. Wiik, S. Aasland, H.L. Hansen, I.L. Tangen, R. Ødegård, Solid State Ionics 152–153 (2002) 675–680.
[35] F. Jin, J. Liu, Y. Shen, T. He, J. Alloys Compd. 685 (2016) 483–491.
[36] Z. Gao, L.V. Mogni, E.C. Miller, J.G. Railsback, S.A. Barnett, Energy Environ. Sci. 9 (2016) 1602–1644.
[37] X. Jiang, Q. Xu, Y. Shi, X. Li, W. Zhou, H. Xu, Q. Zhang, Int. J. Hydrogen Energy 39 (2014) 10817–10823.
[38] S. Lü, X. Meng, X. Fu, M. Liu, Y. Sui, Y. Chen, J. Cao, Y. Sun, Y. Ji, L. Yang, Int. J. Hydrogen Energy 45 (2020) 23227–23236.
[39] K. Takenaka, Sci. Technol. Adv. Mater. 13 (2012) 013001.
[40] F. Lu, M. Yang, Y. Shi, C. Wu, X. Jia, H. He, J. Su, M. Chao, B. Cai, Ceram. Int. 47 (2021) 1095–1100.
[41] L. Hu, D. Zhou, X. Zhu, N. Wang, J. Bai, H. Gong, Y. Zhang, Y. Chen, W. Yan, Q. Zhu, Fuel 362 (2024) 130864.
[42] M. Li, F. Lu, R. Cui, L. Shi, J. Wang, H. He, J. Su, B. Cai, Solid State Ionics 414 (2024) 116639.
[43] D. Heidari, S. Javadpour, S.H. Chan, Energy Convers. Manag. 136 (2017) 78–84.
[44] S.Y. Toor, E. Croiset, Ceram. Int. 46 (2020) 1148–1157.
[45] Y. Zhang, B. Chen, D. Guan, M. Xu, R. Ran, M. Ni, W. Zhou, R. O'Hayre, Z. Shao, Nature 591 (2021) 246–251.
[46] W. Zhou, R. Ran, Z. Shao, W. Jin, N. Xu, J. Power Sources 182 (2008) 24–31.
[47] P. Kim-Lohsoontorn, D.J.L. Brett, N. Laosiripojana, Y.M. Kim, J.M. Bae, Int. J. Hydrogen Energy 35 (2010) 3958–3966.
[48] M. Mori, N.M. Sammes, Solid State Ionics 146 (2002) 301–312.
[49] P. Zeng, R. Ran, Z. Chen, W. Zhou, H. Gu, Z. Shao, S. Liu, J. Alloys Compd. 455 (2008) 465–470.
[50] K.K. Hansen, K.V. Hansen, Solid State Ionics 178 (2007) 1379–1384.
[51] Y. Lin, R. Ran, Y. Zheng, Z. Shao, W. Jin, N. Xu, J. Ahn, J. Power Sources 180 (2008) 15–22.
[52] J. Sun, Z. Zhang, Y. Gong, H. Wang, R. Wang, L. Zhao, B. He, Sci. Rep. 9 (2019) 4210.
[53] L. Ge, W. Zhou, R. Ran, S. Liu, Z. Shao, W. Jin, N. Xu, J. Membr. Sci. 306 (2007) 318–328.
[54] C. Fu, K. Sun, N. Zhang, X. Chen, D. Zhou, Electrochim. Acta 52 (2007) 4589–4594.
[55] M.S. Wang, J.X. Wang, C.R. He, Y.J. Xue, H. Miao, Q. Wang, W.G. Wang, Ceram. Int. 41 (2015) 5017–5025.
[56] X. Ding, X. Kong, J. Jiang, C. Cui, L. Guo, Int. J. Hydrogen Energy 35 (2010) 1742–1748.
[57] X. Fang, J. Zhu, Z. Lin, Energies 11 (2018) 1735.
[58] A. Barbucci, M. Carpanese, A.P. Reverberi, G. Cerisola, M. Blanes, P.L. Cabot, M. Viviani, A. Bertei, C. Nicolella, J. Appl. Electrochem. 38 (2008) 939–945.
[59] M. Juhl, S. Primdahl, C. Manon, M. Mogensen, J. Power Sources 61 (1996) 173–181.
[60] Z. Xie, I. Jang, M. Ouyang, A. Hankin, S.J. Skinner, J. Phys.: Energy 5 (2023) 045005.